An Analysis of the Potential Benefits of Centralised Predictive Control for Optimal Electrical Power Generation from Wave Energy Arrays

Adrian C.M. O'Sullivan, *Student Member, IEEE*, Wanan Sheng and Gordon Lightbody

***Abstract*—This work focuses on an array of point absorbers, with linear permanent magnet generators (LPMG) connected to the grid via back to back voltage source converters, controlled using economic model predictive control (MPC) that produces optimal electrical power generation. The main contribution of this paper is the comparison of the performance provided by using either a centralised or decentralised MPC scheme. In this study, it is shown how the inclusion of viscosity and system constraints limits the benefits to be obtained by the use of a centralised control scheme. Indeed, it was shown that a decentralised MPC scheme was sufficient for the provision of close to optimum electrical power extraction from the array when there was a reasonable separation between WEC devices. It was shown that the introduction of power constraints, either locally at each device or globally for the entire array, improved the quality of the power exported to the grid. Importantly, it was shown that from the viewpoint of power quality, that global predictive control of the wave energy array offered significant benefits over local decentralised control in increasing the average to peak power ratio of power exported to the grid.**

***Index Terms*—Model predictive control; Centralised control; Decentralised control; Average power maximisation; Power quality; Wave energy arrays; Wave to wire.**

I. Introduction

WAVE energy, unlike wind, is an immature technology with many challenges and a wide variety of potential design paradigms, including mechanical/hydrodynamic design, power take off, control and grid integration techniques [1]. A wide range of WEC devices are currently being developed, such as the oscillating water column, the overtopping WEC, the attenuating WEC and the point absorber [2]; it is the last one which is the focus of this paper as it is well suited for deployment in arrays, [3]. Along with hydrodynamic and mechanical design, research has focussed on the problem of the integration of WEC devices into the electricity grid [4]. The electrical system includes generator type [5], cabling [6], safety mechanisms, power conversion, and storage [6], offshore electrical network topologies and whether the network is DC or AC [7]. In WEC design, it is important to focus on the complete wave-to-wire system, to analyse not just the electrical energy harvest, but the quality of the power injected into the electricity grid [6].

A.C.M. O'Sullivan and G. Lightbody are both in MaREI and School of Engineering, University College Cork, College Rd, Co.Cork, Republic of Ireland e-mail: (adrian.osullivan@umail.ucc.ie).

W. Sheng is with MaREI.

This work was supported through the Science Foundation Ireland research centres program, (SFI 12/RC/2302).

Manuscript received August 19, 20; revised October 23, 2017.

By its nature, power quality issues for wave energy devices are significantly more problematic than for wind turbines, with potentially large swings in delivered electrical power occurring over seconds [8]. This is a particular problem for grid integration, specifically when the local grid is weak, which is often likely due to the probable remote locations of WEC systems [9]. One approach is to use energy storage such as batteries or super-capacitors to smooth out the power flow onto the local grid, [6]. Likewise, the aggregation of the electrical power from an array of WECs can be utilised to minimise the resulting significant power fluctuations, simply by nature of their phase differences, or by active control over the array [10].

Ideally, an array should be designed to maximise the electrical energy harvest from a particular site, depending on the wave characteristics of the site including wave direction statistics [11] and the array layout [10]. Recent investigations have found that the inclusion of the control technique in the layout optimisation stage is essential [12] - the control technique, how it is tuned, and the control constraints, all affect the energy extracted from the array.

WEC control techniques initially focussed on linear damping, latching [13], declutching [14], optimal causal control [15] and reactive [16] (impedance matching) control - all of these classical methods have the same objective of maximising average power. However, these typically allow excessive forces to be generated by the power take-off, resulting in significant power swings. Recently, optimal control methods such as bang-bang control [17], dynamic programming [18], pseudospectral control [19] and model predictive control (MPC) [20] have enhanced the extraction of average power from WECs by incorporating design and system constraints into the optimisation process. This present paper utilises Model Predictive Control (MPC), as linear and nonlinear constraints can be easily incorporated [21] in the control design.

Economic MPC was initially introduced to maximise the average mechanical power extracted from a point absorber [20]. Including the resistive losses from the generator in the MPC objective function then allowed for electrical power maximisation [21]. Further developments facilitated the implementation of a nonlinear MPC (NMPC) to maximise average power while considering the nonlinear effects in the system, such as viscosity [22]. Linear mechanical constraints are also commonly used [23], which include limits on heave, velocity and PTO force. Nonlinear constraints are predominantly electrical constraints such as a voltage constraint [21], current limits

(with field weakening) [21], uni-directional power flow [21] and maximum power [24] to protect the power electronics.

Initially, decentralised control was utilised for WEC arrays, where each device is independently controlled, assuming little or no interaction between the devices. Decentralised control techniques for arrays have employed both optimal methods such as MPC [25] and standard methods such as suboptimal control [26]. Optimal centralised methods in which the whole array is controlled as one dynamic system, including the inter-device interactions, have included Galerkin control [27] and MPC [28]. In [27], a comparison between a decentralised and a centralised control system showed that a decentralised control system is sufficient when the separation distance of the devices in the array is over a certain threshold. One key disadvantage of implementing a centralised control system is the computational objective when considering a large array - to overcome this problem distributed control can be used [29]. Distributed control offers performance which comes close to that obtained with centralised control, by the decomposition of the optimisation problem into local problems with some limited communication between the devices [29]. Typically, an iterative MPC method is used which produce an equivalent global solution and which cannot incorporate global constraints [30].

This paper presents a comparison of the maximum electrical energy extraction from arrays of equally spaced point absorbers, utilising both centralised and decentralised MPC control. It focuses on the effect of layout, viscosity and constraints on the potential benefits of a centralised approach. Finally it provides a method for the improvement of electrical power quality through the optimisation process, which is necessary for increasing the bandwidth of the grid-side DC-link voltage controller and to improve flicker.

II. Modelling

The wave to grid electrical system is shown in Fig. 1. The WEC is connected to a linear permanent magnet generator (LPMG) [5], connected to the grid via back to back voltage source converters. The grid side converter is used to control the DC link voltage and reactive power. The machine side converter is used to control the motion of the LPMG. The cables connecting the WECs to the same DC link bus are assumed ideal in this work and are not modelled. Also in this work, the voltage across the DC-link is assumed constant, which decouples the generation side converter from the grid side converter.

A. Hydrodynamics

The two WEC array orientations analysed in this work are shown in Fig. 2. All WECs within the arrays have identical dimensions. The angle of unidirectional wave excitation penetration is θ, and each WEC is equally separated from each other with a separation distance d. Each WEC is restricted to move in the heave direction and its model is based on linear wave theory. The hydrodynamic model of the i^{th} WEC (1), consists of the hydrostatic force $F_{h_i}(t)$, the radiation force

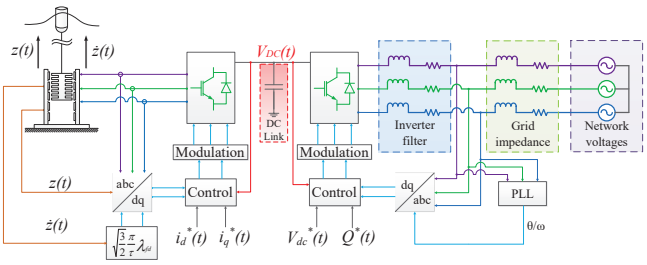

Fig. 1. Schematic of the Wave to Grid electrical system which includes: a point absorber WEC connected to a LPMG, the machine side converter, the machine side controller using dq transformations, the DC-link capacitor, a grid side converter, grid side converter filters, grid impedance network, network voltages, the grid side controller utilising a dq transformation with a PLL.

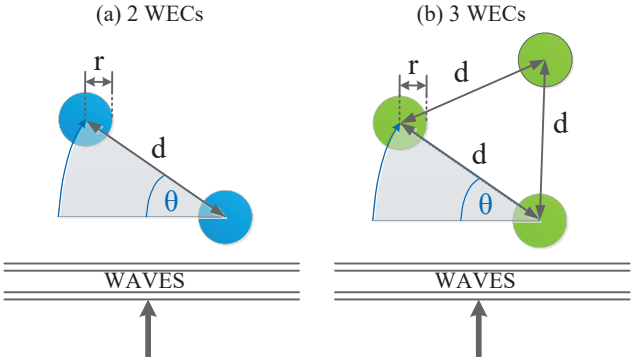

Fig. 2. Top view of (a) a 2 WEC array, (b) a 3 WEC equilateral triangle array with a WEC radius r, a WEC separation distance d, an array orientation θ.

$F_{rad_i}(t)$, the excitation force $F_{e_i}(t)$, the controlled PTO force $F_{PTO_i}(t)$ and the non-linear viscous force $F_{v_i}(t)$,

$$M_i\ddot{z}_i(t) = F_{h_i}(t)+F_{rad_i}(t)+F_{e_i}(t)+F_{PTO_i}(t)+F_{v_i}(t). \quad (1)$$

The hydrodynamic model for a single device (1) is then further developed into (3) where the heave displacement of the i^{th} WEC is $z_i(t)$, the WEC velocity is $\dot{z}_i(t)$, the wave elevation is $\eta_i(t)$ and the wave velocity is $\dot{\eta}_i(t)$. The hydrostatic force $F_{h_i}(t)$ is a function of the displacement $z_i(t)$, where β is the linear hydrostatic spring constant. The radiation force $F_{rad_i}(t)$ is modelled (2) using the Cummins decomposition [31], [32], where the radiation kernels $h_{r_{i,j}}(t)$ and the added mass at infinity frequency m_{μ_i} are found using WAMIT [33].

$$F_{rad_i}(t) = \sum_{j=1}^{N_w}\left[-m_{\mu_{i,j}}\ddot{z}_j(t) + \int_0^t h_{r_{i,j}}(\tau)\dot{z}_j(t-\tau)d\tau\right] \quad (2)$$

The non-linear viscous force $F_{v_i}(t)$ depends on the relative velocity between the WEC and wave and the PTO force $F_{PTO_i}(t)$ is manipulated by the control system,

$$M_i\ddot{z}_i(t) + \sum_{j=1}^{N_w} m_{\mu_{i,j}}\dot{z}_j(t) + \overbrace{\sum_{j=1}^{N_w}\left[\int_0^t h_{r_{i,j}}(\tau)\dot{z}_j(t-\tau)d\tau\right]}^{F_{r_i}(t)}$$
$$+\beta_i z_i(t) + C_{vis_i}(t)\left(\dot{z}_i(t) - \dot{\eta}_i(t)\right) = F_{PTO_i}(t) + F_{e_i}(t). \quad (3)$$

Here N_w is the number of WECs in the array. The excitation force $F_{e_i}(t)$ is a non-causal convolution integral of the wave

elevation $\eta_i(t)$, where the excitation kernel $h_{e_i}(t)$ was found using WAMIT [33],

$$F_{e_i}(t) = \int_{-\infty}^{t} h_{e_i}(\tau)\eta_i(t-\tau)d\tau. \tag{4}$$

The radiation force on the i^{th} WEC, $F_{r_i}(t)$, which is expressed as the sum of forces produced by the movement of the N_w devices in (3), can be realised as a multi-input-single-output state space subsystem (5) using the Hankel singular value decomposition (HSVD) method [34]:

$$\begin{aligned} \dot{\boldsymbol{x}}_{\boldsymbol{r_j}}(t) &= \boldsymbol{A}_{\boldsymbol{r_j}}\boldsymbol{x}_{\boldsymbol{r_j}}(t) + \boldsymbol{B}_{\boldsymbol{r_j}}\dot{z}_j(t) \\ F_{r_i}(t) &= \sum_{j=1}^{N_w}\left(\boldsymbol{C}_{\boldsymbol{r_{i,j}}}\boldsymbol{x}_{\boldsymbol{r_j}}(t) + D_{r_{i,j}}\dot{z}_j(t)\right), \end{aligned} \tag{5}$$

where n is the radiation kernel order, $\boldsymbol{x}_{\boldsymbol{r_j}}(t) \in \mathbb{R}^{n\times 1}$, $\boldsymbol{A}_{\boldsymbol{r_j}} \in \mathbb{R}^{n\times n}$, $\boldsymbol{B}_{\boldsymbol{r_j}} \in \mathbb{R}^{n\times 1}$, $\boldsymbol{C}_{\boldsymbol{r_{i,j}}} \in \mathbb{R}^{1\times n}$, $D_{r_{i,j}} \in \mathbb{R}^1$.

The non-linear viscosity force $F_{v_i}(t)$, is based on the semi-empirical Morison equation [35],

$$F_{v_i}(t) = -C_{vis_i}(t)\left(\dot{z}_i(t) - \dot{\eta}_i(t)\right), \tag{6}$$

where,

$$C_{vis_i}(t) = \frac{1}{2}\rho C_{d_i} A \left|\dot{z}_i(t) - \dot{\eta}_i(t)\right|.$$

Here ρ is the density of water, C_{d_i} is the drag coefficient [36] and A_i is the sectional area of the i^{th} point absorber which is orthogonal to the direction of the force.

Combining all WEC models, a global non-linear hydrodynamic system can be formed, which includes all the cross coupling radiation terms (7), where this system is modelled and simulated using MATLAB/Simulink [37],

$$\frac{d}{dt}\mathbf{X}(t) = \mathbf{A_c}(t)\mathbf{X}(t) + \mathbf{B_c}\mathbf{U_q}(t) + \mathbf{F_c}\mathbf{V}(t) + \mathbf{E_c}(t)\dot{\mathbf{H}}(t). \tag{7}$$

Here,

$$\mathbf{A_c}(t) = \boldsymbol{K_m}^{-1}\begin{bmatrix} \mathbf{A_{c_{1,1}}}(t) & \dots & \mathbf{A_{c_{1,N_w}}}(t) \\ \vdots & \ddots & \vdots \\ \mathbf{A_{c_{N_w,1}}}(t) & \dots & \mathbf{A_{c_{N_w,N_w}}}(t) \end{bmatrix}, \tag{8}$$

$$\mathbf{A_{c_{i,j}}}(t) = \begin{cases} \begin{bmatrix} 0 & 1 & \mathbf{0} \\ -\beta_i & -\Phi_i & -\boldsymbol{C}_{\boldsymbol{r_{i,i}}} \\ 0 & \boldsymbol{B}_{\boldsymbol{r_i}} & \boldsymbol{A}_{\boldsymbol{r_i}} \end{bmatrix}, & \text{if } i = j \\ \begin{bmatrix} 0 & 0 & \mathbf{0} \\ +0 & -D_{r_{i,j}} & -\boldsymbol{C}_{\boldsymbol{r_{i,j}}} \\ 0 & \boldsymbol{B}_{\boldsymbol{r_j}} & \boldsymbol{A}_{\boldsymbol{r_j}} \end{bmatrix}, & \text{if } i \neq j \end{cases},$$

where $\mathbf{A_c}(t) \in \mathbb{R}^{N_w(n+2)\times N_w(n+2)}$, $A_{c_{i,j}}(t) \in \mathbb{R}^{(n+2)\times(n+2)}$ and $\Phi_i = (D_{r_{i,i}} + C_{vis_i}(t))$,

$$\mathbf{B_c} = \boldsymbol{K_m}^{-1}\begin{bmatrix} \boldsymbol{B}_{\boldsymbol{c_1}} & \dots & \mathbf{0} \\ \vdots & \ddots & \vdots \\ \mathbf{0} & \dots & \boldsymbol{B}_{\boldsymbol{c_{N_w}}} \end{bmatrix},$$

$$\mathbf{F_c} = \boldsymbol{K_m}^{-1}\begin{bmatrix} \boldsymbol{F}_{\boldsymbol{c_1}} & \dots & \mathbf{0} \\ \vdots & \ddots & \vdots \\ \mathbf{0} & \dots & \boldsymbol{F}_{\boldsymbol{c_{N_w}}} \end{bmatrix},$$

$$\mathbf{E_c}(t) = \boldsymbol{K_m}^{-1}\begin{bmatrix} \boldsymbol{E}_{\boldsymbol{c_1}}(t) & \dots & \mathbf{0} \\ \vdots & \ddots & \vdots \\ \mathbf{0} & \dots & \boldsymbol{E}_{\boldsymbol{c_{N_w}}}(t) \end{bmatrix}, \tag{9}$$

$$\boldsymbol{B}_{\boldsymbol{c_i}} = \boldsymbol{F}_{\boldsymbol{c_i}} = \boldsymbol{K_m}^{-1}\begin{bmatrix} 0 \\ (M_i + m_{\mu_i}) \\ \mathbf{0} \end{bmatrix} \in \mathbb{R}^{(n+2)\times 1},$$

$$\boldsymbol{E}_{\boldsymbol{c_i}}(t) = \boldsymbol{K_m}^{-1}\begin{bmatrix} 0 \\ C_{vis_i}(t) \\ \mathbf{0} \end{bmatrix} \in \mathbb{R}^{(n+2)\times 1},$$

where $\mathbf{B_c} \in \mathbb{R}^{N_w(n+2)\times N_w}$, $\mathbf{F_c} \in \mathbb{R}^{N_w(n+2)\times N_w}$, $\mathbf{E_c}(t) \in \mathbb{R}^{N_w(n+2)\times N_w}$

$$\boldsymbol{K_m} = \begin{bmatrix} \boldsymbol{M}_{\boldsymbol{a_{1,1}}} & \dots & \boldsymbol{M}_{\boldsymbol{a_{1,N_w}}} \\ \vdots & \ddots & \vdots \\ \boldsymbol{M}_{\boldsymbol{a_{N_w,1}}} & \dots & \boldsymbol{M}_{\boldsymbol{a_{N_w,N_w}}} \end{bmatrix} \tag{10}$$

$$\boldsymbol{M}_{\boldsymbol{a_{i,j}}} = \begin{cases} \begin{bmatrix} 1 & 0 & \mathbf{0} \\ 0 & (M_i + m_{\mu_{i,i}}) & \mathbf{0} \\ \mathbf{0} & \mathbf{0} & \mathbf{I} \end{bmatrix}, & \text{if } i = j \\ \begin{bmatrix} 0 & 0 & \mathbf{0} \\ 0 & m_{\mu_{i,j}} & \mathbf{0} \\ \mathbf{0} & \mathbf{0} & \mathbf{0} \end{bmatrix}, & \text{if } i \neq j \end{cases}$$

where $\boldsymbol{K_m} \in \mathbb{R}^{N_w(n+2)\times N_w(n+2)}$, $\boldsymbol{M}_{\boldsymbol{a_{i,j}}} \in \mathbb{R}^{(n+2)\times(n+2)}$,

$$\begin{aligned} \mathbf{X}(t) &= \begin{bmatrix} \boldsymbol{x_1(t)} \\ \vdots \\ \boldsymbol{x}_{\boldsymbol{N_w}}(t) \end{bmatrix}, \mathbf{U_q}(t) = \begin{bmatrix} u_{q_1}(t) \\ \vdots \\ u_{q_{N_w}}(t) \end{bmatrix}, \\ \mathbf{V}(t) &= \begin{bmatrix} v_1(t) \\ \vdots \\ v_{N_w}(t) \end{bmatrix}, \dot{\mathbf{H}}(t) = \begin{bmatrix} \dot{\eta}_1(t) \\ \vdots \\ \dot{\eta}_{N_w}(t) \end{bmatrix}, \\ \boldsymbol{x}_i(t) &= \begin{bmatrix} z_i(t) \\ \dot{z}_i(t) \\ \boldsymbol{x}_{\boldsymbol{r}i}(t) \end{bmatrix}. \end{aligned} \tag{11}$$

Here $\boldsymbol{x}_i(t) \in \mathbb{R}^{(n+2)\times 1}$, $\mathbf{X}(t) \in \mathbb{R}^{N_w(n+2)\times 1}$ and $\{\mathbf{U_q}(t), \mathbf{V}(t), \dot{\mathbf{H}}(t)\} \in \mathbb{R}^{N_w\times 1}$ and the scaled forces, $u_{q_i}(t)$ and $v_i(t)$ are,

$$u_{q_i}(t) = \frac{F_{PTO_i}(t)}{M_i + m_{\mu_i}} \qquad v_i(t) = \frac{F_{e_i}(t)}{M_i + m_{\mu_i}} \tag{12}$$

III. Control

In this work, a cascade controller is used for each localised WEC system, as shown in Fig. 3. An economic model predictive control (MPC) controller is implemented on the outer slower loop, which maximises the average electrical power extracted from the system. Using the optimum LPMG force set point $u_{q_i}(k)$ provided from the outer loop, the faster inner loop produces this LPMG force utilising PI control, where the PWM is modelled as a time delay. Here zero field weakening is assumed ($i_{d_i}(t) = 0$ A), [21].

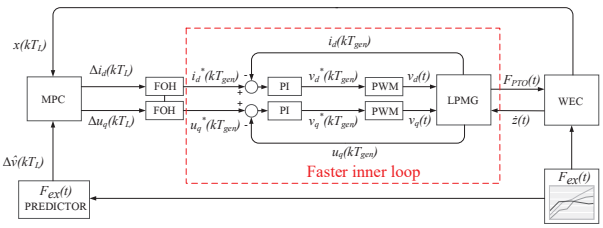

Fig. 3. Cascade control scheme of slower MPC outer loop and faster LPMG PTO force controller.

A. The Objective Function

The purpose of the MPC presented in this work is to maximise the electrical power absorbed from the entire WEC array. The total average electrical power absorbed from the array can be expressed as (13),

$$P_{e_{tot}}(t) = \sum_{i=1}^{N_w} P_{e_i}(t). \tag{13}$$

Here each individual WEC average electrical power $P_{e_i}(t)$ can be determined as (14),

$$P_{e_i} = -\frac{1}{T}\int_{t=0}^{T}\left(\left(M_i + m_{\mu_i}\right)u_{q_i}(t)\dot{z}_i(t) + \frac{R}{\psi^2}u_{q_i}^2(t)\right)dt. \tag{14}$$

where R is the LPMG resistance and as shown in [21],

$$\psi = \frac{\frac{\pi}{\tau}\lambda_{fd}^{'}}{\left(M_i + m_{\mu_i}\right)}$$

Here τ is the pole pitch and $\lambda_{fd}^{'}$ is the scaled flux linkage of the LPMG. In this paper, as in previous work [21], the outer MPC loop in the cascade control scheme sends optimal $u_{q_i}(t)$ ramp trajectories to the inner current control loop which operates at a much higher bandwidth. Since a first order hold (FOH) is utilised, $u_{q_i}(k)$ and $\dot{z}_i(k)$ are both piecewise linear between the outer-loop samples and the average electrical power for a single WEC (14) can be estimated in the discrete domain using trapezoidal integration. Maximising electrical power P_{e_i} for the i^{th} WEC is equivalent to minimising the objective function $J_i(k)$, (15),

$$J_i(k) = \frac{1}{2}u_{q_i}(k+N)\dot{z}_i(k+N) + \sum_{j=1}^{N-1}u_{q_i}(k+j)\dot{z}_i(k+j) + \frac{R(M_i+m_{\mu_i})}{(\lambda_{fd}^{'}\frac{\pi}{\tau})^2}\left(\frac{1}{2}u_{q_i}^2(k+N) + \sum_{j=1}^{N-1}u_{q_i}^2(k+j)\right). \tag{15}$$

Combining the N_w local objective functions (15), a global objective function is formed (16),

$$J_T(k) = \sum_{i=1}^{N_w} J_i(k). \tag{16}$$

Using optimisation algorithms such as quadratic programming (QP) over a prediction horizon N, the objective function (16) can be minimised.

B. Non-linear Model Predictive Control

If initially an inviscid hydrodynamic system (6) is assumed ($C_d = 0$), then a discrete time-invariant MPC prediction model of the array can be used [21]. However, when viscosity is included in the system model, a non-linear MPC (NMPC) is utilised [22], which employs a discrete time-variant model (20). The NMPC required the predicted velocities obtained from the solution to the optimal control problem at the last control sample, where the non-linear viscous coefficient can then be linearised at each control sample (17) across the prediction horizon. This converts a non-linear problem into a discrete time-varying linear optimal problem.

$$\tilde{\boldsymbol{C}}_{\boldsymbol{vis_i}}(k+j) = \rho C_{d_i} A\left|\dot{\boldsymbol{z}}_{\boldsymbol{i}}^{*}(k+j|k-1) - \dot{\boldsymbol{\eta}}_{\boldsymbol{i}}(k+j))\right| \tag{17}$$

where $j \in \{0,\ldots,(N-1)\}$ and $j = i \in \{1,\ldots,N_w\}$, $\tilde{\boldsymbol{C}}_{\boldsymbol{vis_i}}(k+j) \in \mathbb{R}^{N\times 1}$ and $\dot{\boldsymbol{z}}_{\boldsymbol{i}}^{*}(k+j|k-1)$ is the predicted velocity at the j^{th} step into the future for the i_{th} WEC device, from the optimal state trajectory predicted as part of the solution for the controls at the $(k-1)^{th}$ sample. It is assumed here that the sea surface velocity for the i_{th} WEC device $\dot{\boldsymbol{\eta}}_{\boldsymbol{i}}(k+j)$ is known over the prediction horizon.

Using these predicted velocities, $\dot{\boldsymbol{z}}_{\boldsymbol{i}}^{*}(k+j|k-1)$ and $\dot{\boldsymbol{\eta}}_{\boldsymbol{i}}(k+j)$, the non-linear $\mathbf{A_c}(t)$ (8) and $\mathbf{E_c}(t)$ (9) matrices can then be linearised at each control step over the horizon, as shown in (18) and (19),

$$\tilde{\mathbf{A}}_{\mathbf{c}}(k+j) = \boldsymbol{K_m}^{-1}\begin{bmatrix}\tilde{\mathbf{A}}_{\mathbf{c_{1,1}}}(k+j) & \ldots & \tilde{\mathbf{A}}_{\mathbf{c_{1,N_w}}} \\ \vdots & \ddots & \vdots \\ \tilde{\mathbf{A}}_{\mathbf{c_{N_w,1}}} & \ldots & \tilde{\mathbf{A}}_{\mathbf{c_{N_w,N_w}}}(k+j)\end{bmatrix},$$

$$\tilde{\mathbf{A}}_{\mathbf{c_{i,i}}}(k+j) = \begin{bmatrix}0 & 1 & \mathbf{0} \\ -\beta_i & -\Phi_i(k+j) & -\boldsymbol{C}_{\boldsymbol{r_{i,i}}} \\ 0 & \boldsymbol{B}_{\boldsymbol{r_i}} & \boldsymbol{A}_{\boldsymbol{r_i}}\end{bmatrix}, \tag{18}$$

$$\tilde{\mathbf{E}}_{\mathbf{c}}(k+j) = \boldsymbol{K_m}^{-1}\begin{bmatrix}\tilde{\boldsymbol{E}}_{\mathbf{c_1}}(k+j) & \ldots & \mathbf{0} \\ \vdots & \ddots & \vdots \\ \mathbf{0} & \ldots & \tilde{\boldsymbol{E}}_{\boldsymbol{c_{N_w}}}(k+j)\end{bmatrix},$$

$$\tilde{\mathbf{E}}_{\mathbf{c_i}}(k+j) = \begin{bmatrix}0 \\ \tilde{\boldsymbol{C}}_{\boldsymbol{vis_i}}(k+j) \\ \mathbf{0}\end{bmatrix}, \tag{19}$$

Assuming a first-order hold (FOH) and integral action, the discretisation of the time-variant continuous model results in the following discrete time, LPV prediction model,

$$\mathbf{X_f}(k+j+1) = \mathbf{A_f}(k+j)\mathbf{X_f}(k+j) + \mathbf{B_f}(k+j)\boldsymbol{\Delta}\mathbf{U_q}(k+j+1) + \mathbf{F_f}(k+j)\boldsymbol{\Delta}\mathbf{V}(k+j+1) + \mathbf{E_f}(k+j)\boldsymbol{\Delta}\dot{\mathbf{H}}(k+j+1) \tag{20}$$

$$\mathbf{Y_f}(k+j) = \mathbf{C_f}\mathbf{X_f}(k+j),$$

and

$$\mathbf{X_f}(k+j) = \begin{bmatrix} \mathbf{X}(k+j) \\ \dot{\mathbf{U}}_\mathbf{q}(k+j) \\ \mathbf{V}(k+j) \\ \dot{\mathbf{H}}(k+j) \end{bmatrix} \in \mathbb{R}^{N_w(n+5)\times 1}$$

$$\mathbf{Y_f}(k+j) = \begin{bmatrix} z_1(k+j) \\ \dot{z}_1(k+j) \\ u_{q1}(k+j) \\ \vdots \\ z_{N_w}(k+j) \\ \dot{z}_{N_w}(k+j) \\ u_{qN_w}(k+j) \end{bmatrix} \in \mathbb{R}^{3N_w\times 1}$$

$$\mathbf{A_f}(k+j) = \begin{bmatrix} e^{\tilde{\mathbf{A}}_\mathbf{c}(k+j)T_L} & \mathbf{\Lambda_B}(k+j) & \mathbf{\Lambda_B}(k+j) & \mathbf{\Lambda_V}(k+j) \\ \mathbf{0} & \mathbf{I} & \mathbf{0} & \mathbf{0} \\ \mathbf{0} & \mathbf{0} & \mathbf{I} & \mathbf{0} \\ \mathbf{0} & \mathbf{0} & \mathbf{0} & \mathbf{I} \end{bmatrix}$$

Here $\mathbf{A_f}(k+j) \in \mathbb{R}^{N_w(n+5)\times N_w(n+5)}$,

$\mathbf{\Lambda_B}(k+j) = \tilde{\mathbf{A}}_\mathbf{c}(k+j)^{-1}\left(e^{\tilde{\mathbf{A}}_\mathbf{c}(k+j)T_L} - \mathbf{I}\right)\mathbf{B_c}$,

$\mathbf{\Lambda_V}(k+j) = \tilde{\mathbf{A}}_\mathbf{c}(k+j)^{-1}\left(e^{\tilde{\mathbf{A}}_\mathbf{c}(k+j)T_L} - \mathbf{I}\right)\tilde{\mathbf{E}}_\mathbf{c}(k+j)$.

Then using the linear approximation $\tilde{\mathbf{E}}_\mathbf{c}(k+j)$ from (19), the following can be constructed,

$$\mathbf{B_b}(k+j) = \begin{bmatrix} \mathbf{\Gamma_B}(k+j) \\ \mathbf{I} \\ \mathbf{0} \\ \mathbf{0} \end{bmatrix} \in \mathbb{R}^{N_w(n+5)\times 1}$$

$$\mathbf{F_b}(k+j) = \begin{bmatrix} \mathbf{\Gamma_B}(k+j) \\ \mathbf{0} \\ \mathbf{I} \\ \mathbf{0} \end{bmatrix} \in \mathbb{R}^{N_w(n+5)\times 1}$$

$$\mathbf{E_b}(k+j) = \begin{bmatrix} \mathbf{\Gamma_V}(k+j) \\ \mathbf{0} \\ \mathbf{0} \\ \mathbf{I} \end{bmatrix} \in \mathbb{R}^{N_w(n+5)\times 1}$$

where, $\mathbf{\Gamma_B}(k+j) = \frac{1}{T_L}\tilde{\mathbf{A}}_\mathbf{c}(k+j)^{-1}\left(\mathbf{\Lambda_B}(k+j) - T_L\mathbf{B_c}\right)$,

$\mathbf{\Gamma_V}(k+j) = \frac{1}{T_L}\tilde{\mathbf{A}}_\mathbf{c}(k+j)^{-1}\left(\mathbf{\Lambda_V}(k+j) - T_L\tilde{\mathbf{E}}_\mathbf{c}(k+j)\right)$.

Assuming that the future excitation wave forces are known over the prediction horizon, the output vector of the system can be predicted over the N step prediction horizon using (21),

$$\hat{\mathbf{Y}}_\mathbf{f}(k) = \mathbf{P}\mathbf{X_f}(k) + \mathbf{H_a}\mathbf{\Delta}\hat{\mathbf{U}}_\mathbf{q}(k) + \mathbf{H_w}\mathbf{\Delta}\hat{\mathbf{V}}(k) + \mathbf{H}_\eta\mathbf{\Delta}\hat{\dot{\mathbf{H}}}(\mathbf{k}), \tag{21}$$

where

$$\hat{\mathbf{Y}}_\mathbf{f}(k) = \begin{bmatrix} \mathbf{Y_f}(k+1|k) \\ \vdots \\ \mathbf{Y_f}(k+N|k) \end{bmatrix} \in \mathbb{R}^{N(3N_w)\times 1} \tag{22}$$

and $\mathbf{P} \in \mathbb{R}^{N(3N_w)\times(n+4)N_w}$, $\mathbf{H_a} \in \mathbb{R}^{N(3N_w)\times N(N_w)}$, $\mathbf{H_w} \in \mathbb{R}^{N(3N_w)\times N(N_w)}$, $\mathbf{H}_\eta \in \mathbb{R}^{N(3N_w)\times N(N_w)}$, $\mathbf{\Delta}\hat{\mathbf{U}}_\mathbf{q}(k) \in \mathbb{R}^{N(N_w)\times 1}$, $\mathbf{\Delta}\hat{\mathbf{V}}(k) \in \mathbb{R}^{N(N_w)\times 1}$, $\mathbf{\Delta}\hat{\dot{\mathbf{H}}}(k) \in \mathbb{R}^{N(N_w)\times 1}$; a full description of these matrices structures is provided in [22].

Using the output predictions (22), the objective function (16) can then be represented in matrix form (23),

$$J_T(k) = \frac{1}{2}\hat{\mathbf{Y}}_\mathbf{f}(k)^T\mathbf{Q_a}\hat{\mathbf{Y}}_\mathbf{f}(k), \tag{23}$$

where,

$$\mathbf{Q_a} = \begin{bmatrix} \mathbf{Q}_1 & \dots & \mathbf{0} \\ \vdots & \ddots & \vdots \\ \mathbf{0} & \dots & \mathbf{Q}_{N_w} \end{bmatrix} \in \mathbb{R}^{N(3N_w)\times N(3N_w)}.$$

Here $\mathbf{Q}_i \in \mathbb{R}^{3N\times 3N}$ and $\mathbf{\Psi}_i \in \mathbb{R}^{3\times 3}$,

$$\mathbf{Q}_i = \begin{bmatrix} \mathbf{\Psi}_i & \dots & \mathbf{0} \\ \vdots & \ddots & \vdots \\ \mathbf{0} & \dots & \frac{1}{2}\mathbf{\Psi}_i \end{bmatrix}, \ \mathbf{\Psi}_i = \begin{bmatrix} 0 & 0 & 0 \\ 0 & 0 & 1 \\ 0 & 1 & 2G_i \end{bmatrix}$$

and

$$G_i = \frac{R(M_i + m_{\mu_i})}{(\lambda'_{fd}\frac{\pi}{\tau})^2}.$$

Neglecting terms that are independent of $\mathbf{\Delta}\mathbf{U_q}(k)$, the expansion of (23) yields (24),

$$\begin{aligned} J_T(k) = {} & \frac{1}{2}\mathbf{\Delta}\hat{\mathbf{U}}_\mathbf{q}{}^T\mathbf{H_a}{}^T\mathbf{Q_a}\mathbf{H_a}\mathbf{\Delta}\hat{\mathbf{U}}_\mathbf{q} \\ & + \mathbf{\Delta}\hat{\mathbf{U}}_\mathbf{q}{}^T\mathbf{H_a}{}^T\mathbf{Q_a}\left(\mathbf{P}\mathbf{X_f} + \mathbf{H_w}\mathbf{\Delta}\hat{\mathbf{V}} + \mathbf{H}_\eta\mathbf{\Delta}\hat{\dot{\mathbf{H}}}\right). \end{aligned} \tag{24}$$

The LPMG resistance term R acts as an extra weight term in the objective function (24), where the objective function that was previously not semi-positive definite is converted into a semi-definite problem [38]. Quadratic programming (QP) solvers, such as in MATLAB or AMPL [39], can be used to minimise the objective function across a prediction horizon, subject to constraints.

C. System Constraints

In this work both mechanical linear constraints and an electrical non-linear constraint are assumed. The mechanical linear constraints that are applied to the each individual WEC consist of heave displacement, WEC velocity and PTO force, as shown in [21]. The non-linear constraint that is applied to the array is a peak electrical power limit. In this work, both local and global peak power constraints are applied to show the potential benefits of electrical power balancing.

The local peak power constraint (25) is defined as,

$$P_{st_i}(k+j) \leq P_{MAX_i}, \tag{25}$$

and the global peak power constraint (26) is defined as,

$$\sum_{i=1}^{N_w} P_{st_i}(k+j) \leq P_{MAX}, \tag{26}$$

where $P_{st_i}(k+j)$ is the instantaneous power for the i^{th} WEC (27), $i \in \{1,\dots,N_w\}$ and $j \in \{1,\dots,N\}$.

$$\begin{aligned} & P_{st_i}(k+j) = \\ & \left(M_i + m_{\mu_{i,i}}\right)u_{q_i}(k+j)\dot{z}_i(k+j) + \frac{R}{\psi^2}u_{q_i}^2(k+j). \end{aligned} \tag{27}$$

D. Move-blocking Control Horizon

An economic MPC controller typically uses a control horizon of the same size as the prediction horizon, $N_c = N$. However, the computational burden can be lowered by utilising move-blocking, while maintaining the fidelity of an MPC with a full control horizon ($N_c = N$) [40].The move-blocking control horizon spreads the N_c control variables appropriately across the prediction horizon N, where the control variables are concentrated over the early stages of the prediction horizon. The early control variables allow faster control action and constraint feasibility while the remainder of the control variables are used to estimate the power over the prediction horizon. The move-blocking control horizon for the i^{th} WEC, $\boldsymbol{\Delta u_{b_i}}(k)$, is defined as the follow,

$$\boldsymbol{\Delta u_{b_i}}(k) = \begin{bmatrix} \boldsymbol{\Xi}_1 & \dots & \mathbf{0} \\ \vdots & \ddots & \vdots \\ \mathbf{0} & \dots & \boldsymbol{\Xi}_{N_c} \end{bmatrix} \boldsymbol{\Delta u_{q_i}}(k)$$

where $\boldsymbol{\Delta u_{b_i}}(k) \in \mathbb{R}^{N_c \times 1}$,

$$\boldsymbol{\Xi}_j = \begin{bmatrix} \mathbf{1}_{\boldsymbol{\varphi}_j \times 1} & \mathbf{0}_{\boldsymbol{\varphi}_j \times (\boldsymbol{\varphi}_j - 1)} \end{bmatrix} \in \mathbb{R}^{\varphi_j \times \varphi_j},$$

$$\boldsymbol{\Delta u_{q_i}}(k) = \begin{bmatrix} \Delta u_{q_i}(k+1) \\ \vdots \\ \Delta u_{q_i}(k+N) \end{bmatrix} \in \mathbb{R}^{N \times 1},$$

where matrix $\boldsymbol{\varphi} \in \mathbb{R}^{N_c \times 1}$ is a predeclared array that designates the concentration of control variables and $\sum_{j=1}^{N_c} \boldsymbol{\varphi}_j = N$.

IV. Results

The WEC used in this research is a cylindrical point absorber with a semi-hemispherical bottom [21], modelled using the following parameters in Table I. The added mass $m_{\mu_{i,j}}$, and the radiation system order ($n \in \{5, \dots, 9\}$), depend on the separation distance between each WEC.

TABLE I
Individual System Values

	Parameters	Units	Value
WEC radius	r	m	5
WEC draft	d_r	m	10
Hydrostatic coefficient	β	kg/s^2	7.89×10^5
Viscous drag coefficient	C_d		1.8
LPMG resistance	R	Ω	0.27
LPMG scaled flux linkage	λ'_{fd}	Wb	$\sqrt{\frac{3}{2}}46$
LPMG tooth pitch	τ	m	0.1

A. Centralised Predictive Control of Wave Energy Arrays

The effects of incorporating linear constraints in the centralised MPC (24) is explored. The linear constraints include the heave displacement $\pm z_{max}$, the heave velocity $\pm \dot{z}_{max}$ and the scaled PTO force $\pm u_{q_{max}}$. Subsequently the effect of viscosity on the array interactions is then analysed using a non-linear MPC (NMPC) where the viscous force $F_v(t)$ was discussed in section II-A. The structure and algorithm of this NMPC is thoroughly discussed in [22], where the predicted states over the prediction horizon of the NPMC are dependent on the previously predicted wave and WEC velocities.

1) The Effect of Constraints and Viscosity on the Sensitivity of the Array Power to Changes in Penetration Angle: In this section the unconstrained system was excited with 1 m high monochromatic waves with wave frequencies $\omega \in \{0.6, \dots 1.22\}$ rad/s and a range of penetration angles $\theta \in \{0, \dots 2\pi\}$ rad. The power variance factor $\Delta P^2(\omega)$ is defined in (28),

$$\Delta P^2(\omega) = \frac{\sum_{\theta} \left[\bar{P}(\theta, \omega) - \bar{P}_\theta(\omega)\right]^2}{N_\theta}. \tag{28}$$

Here $\Delta P^2(\omega)$ is a measure of how much the average power varies with the wave penetration angle range θ. $\bar{P}(\theta, \omega)$ is the average power of the array with a specific orientation θ and wave frequency ω. $\bar{P}_\theta(\omega)$ is the mean average power of the array across the θ range for excitation frequency ω. The power variance factor $\Delta P^2(\omega)$ is then averaged over the N_θ possible penetration angle as shown in (28).

The constrained system was initially excited with 1 m high monochromatic waves with wave frequencies $\omega \in \{0.6, \dots 1.22\}$ rad/s. To simplify the analysis, the two device array orientation was chosen with a constant separation distance of $d = 25$m. In Fig. 4, the power variance factor $\Delta P^2(\omega)$ across the θ range ($\theta \in \{0, \dots 2\pi\}$ rad) is shown for each frequency.

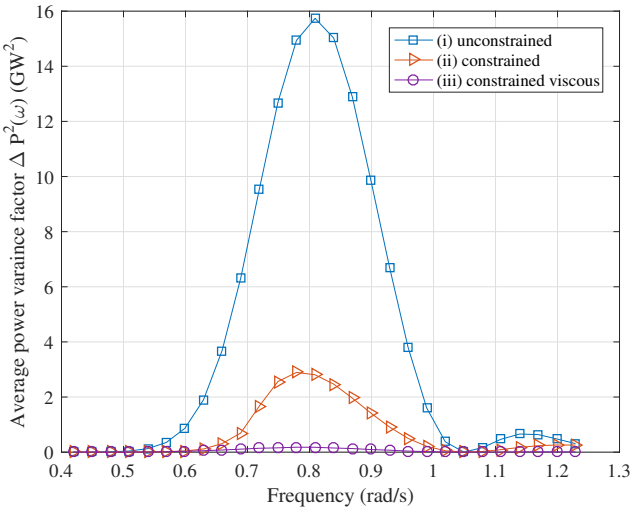

Fig. 4. The power variance factor $\Delta P^2(\omega)$ of the average power $\bar{P}$ absorbed from a fully coupled two device WEC array receiving $\alpha = 1$ m high monochromatic waves across a range of $\theta \in \{0, \dots 2\pi\}$ at a constant separation distance of $d = 25$ m when (i) an unconstrained global MPC controller is used, (ii) a constrained global MPC controller is used and when (iii) a constrained non-linear global MPC controller is used which includes the effects of viscosity

The results in Fig. 4 show that when linear constraints are incorporated into the NMPC, which is implemented on a viscous system, the variance of the average power dramatically reduces; this results in an array with reduced constructive and destructive interactions. The inclusion of the mechanical linear constraints restricts the WEC's heave motion. When implementing the NMPC, which optimises for maximum power absorption from a viscid system, the relative velocity between the WEC and wave surface is inherently reduced, causing a reduction in waves radiated towards neighbouring WECs.

2) The Effect of Constraints and Viscosity on the q Factor of the Array: In this section the q factor (29) of the array is analysed, where the q factor is a ratio of the average power extracted from a coupled array $\bar{P}_c(\omega,\theta)$ to the average power extracted from an array of N_w isolated identical WECs each producing $\bar{P}_d(\omega,\theta)$,

$$q(\omega,\theta) = \frac{\bar{P}_c(\omega,\theta)}{N_w \bar{P}_d(\omega,\theta)}. \tag{29}$$

The constrained system was excited with 1 m high monochromatic waves. As in section. IV-A1, the two device array orientation was chosen with a constant separation distance of $d = 25$m to simplify the analysis. The frequencies $\omega \in \{0.6, \ldots 1.22\}$ rad/s and the penetration angle $\theta \in \{0, \ldots 2\pi\}$ rads where uniformly distributed. The results shown in Fig. 5 presents the minimum, average and maximum q factor across the range of ω and θ values. It is evident that as the linear constraints are included into the MPC, the maximum and minimum q factor values each move closer to unity. As the viscosity force $F_v(t)$ is then included in the system and the linear constraints are included in the NMPC, the minimum and maximum q factors move even closer to unity. It is clearly shown in Fig. 5 that both the presence of constraints and viscosity lead to a reduction in the variability of the q factor in response to the penetration angle and frequency. This also signifies that the effects of constructive and destructive interactions diminish.

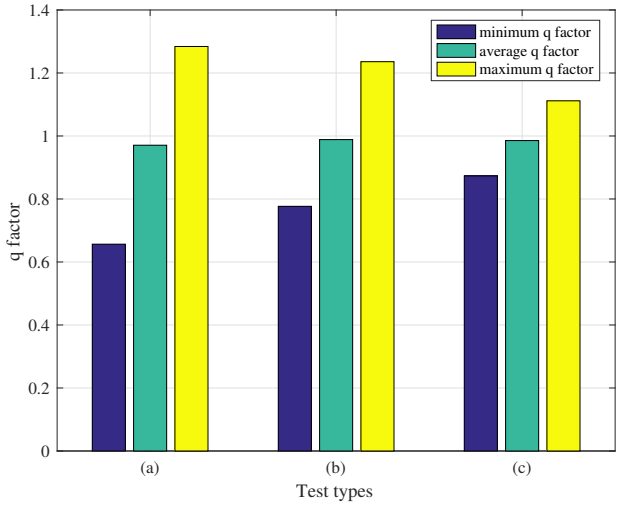

Fig. 5. The q factor range (minimum, average, maximum) from a fully coupled two device WEC array receiving high monochromatic waves with a range of equally distributed wave penetration angles $\theta \in \{0, \ldots 2\pi\}$ rad and frequencies $\omega \in \{0.4, \ldots 1.22\}$ rad.s^{-1} at a constant separation distance of $d = 25$ m when (a) an unconstrained global MPC controller is used, (b) a constrained global MPC controller is used and when (c) a constrained non-linear global MPC controller is used which includes the effects of viscosity

B. Centralised vs Decentralised Predictive Control

The NMPC is used here, including both viscosity and mechanical constraints. The array in each case is excited with irregular wave obeying the Bretschneider spectrum. Three sea states are examined, ($T_p = 6$ s, $H_s = 1$ m), ($T_p = 7.8$ s, $H_s = 2$ m) and ($T_p = 9.6$ s, $H_s = 3$ m). The waves are unidirectional, with a penetration angle $\theta = \pi/4$ rad. The performance of a centralised, and a decentralised NMPC are compared for the following range of separation distance to WEC radius $d/r \in \{3, 5, 8, 12\}$. In the centralised NMPC, the full model of the array including the interactions between devices is used - the power extracted using this control is P_{global}. In the decentralised NMPC, the problem is broken down into N_w simpler independent control problems, one for each device, assuming that there is no interaction between the devices in the array - the power extracted from the array is P_{local}.

Fig. 6 shows the power ratio P_{local}/P_{global} for both a two device and a three device array, for these sea-states, and how this depends on d/r. Indeed it is apparent that for reasonable device separation for both arrays, that there is little benefit to be obtained from using a centralised over a decentralised controller. For separation ratio $d/r > 5$ for the two device array and $d/r > 7$ for the three device array, the decentralised MPC extracts $> 99\%$ of the global optimum electrical power, over the three sea states.

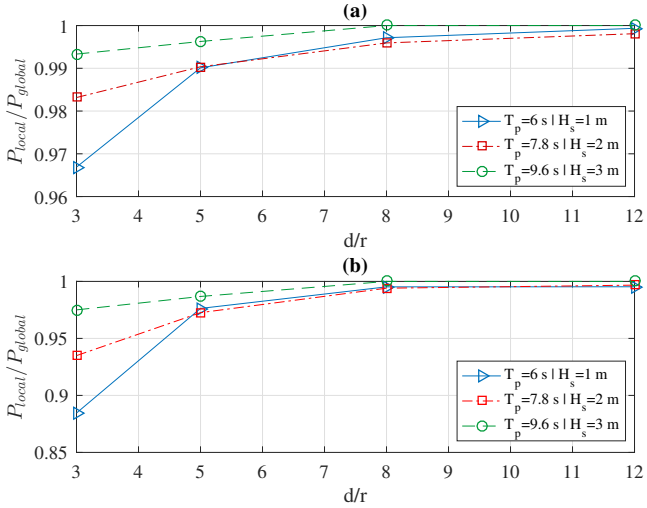

Fig. 6. The average power ratio produced between the decentralised MPC P_{local} and the centralised MPC P_{global} for three unidirectional irregular sea states. The wave penetration angle is $\theta = \pi/4$ rad and the range of (separation/WEC radii) distances $d/r \in \{3, 5, 8, 12$ m$\}$ where (a) two device array, (b) three device array

C. Control of the Electrical Power Quality

Even though the maximisation of the average power from the WEC array is desirable, another primary problem which is frequently highlighted is the low average to peak power ratio from the extracted instantaneous power. Ideally, the instantaneous power exported from the WEC array onto the grid should be constant, especially at high power levels where high power fluctuations may cause stability problems in weak grids. The instantaneous power extracted from a wave energy device is generally an oscillatory waveform. Aggregating the power from multiple devices could decrease the variability of the power exported to the grid, due to the fact that the WEC devices each receive different excitation waves, hence each producing power waveforms may be are out of phase.

In this section an upper instantaneous power limit P_{MAX} is incorporated into the centralised NMPC; this is compared with

the results obtained when applying a local power constraint P_{MAX}/N_w to each individual device. Also incorporated in both the global and local power constrained NMPC is a move-blocking technique [40], which reduces the computational effort of the QP algorithm while maintaining a similar performance to an economic MPC with a full horizon; in this case the selected move-blocking horizon is $N_c = 40$. As shown in section IV-B, when an irregular excitation wave with sea state 3 ($T_p = 9.6$ s and $H_s = 3$ m) was implemented on the two arrays, the difference between the centralised control system and the decentralised control system was insignificant. In this analysis a three WEC array with a set wave penetration angle $\theta = \pi/4$ rad and separation distance of $d = 40$ m ($d/r = 8$) is chosen, as it is the threshold in Fig. 6(b) where the P_{local}/P_{global} ratio is effectively unity. The analysis consists of simulating the system under the same irregular sea state waveforms with a range of different instantaneous power limits for the array $P_{MAX} \in \{0.25,\ 0.5,\ 0.75,\ 1,\ 1.5,\ 2,\ 3,\ 4,\ 5,\ 6\}$ MW.

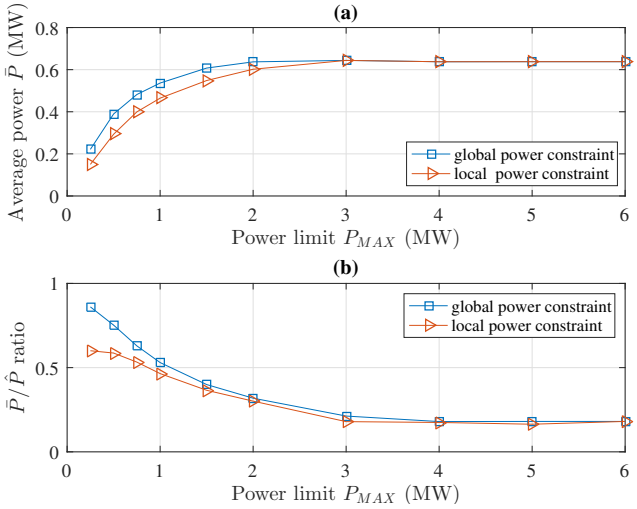

Fig. 7. An analysis of the power extracted from a three device array with either global power constraint or a local power constraint with a unidirectional irregular sea state modelled using a Bretschneider spectrum with $H_s = 3$ m and $T_s = 9.6$ s (a) Average absorbed power $\bar{P}$ from the entire three WEC array, (b) the average to peak power ratio $\bar{P}/\hat{P}$ of the entire three WEC array

It is shown in Fig. 7(a) that as the array power limit P_{MAX} decreases, the average power $\bar{P}$ extracted decreases. It is noticeable that the average power from the global power limited system is greater than the average power using the local power constraint. From Fig. 7(b), it is important to note that for the global power constraint that the average to peak ratio $\bar{P}/\hat{P}$ when the power is constrained is superior to the value found with local device power limits.

For example, in Fig. 7(b) when the power limit is $P_{MAX} = 0.25$ MW, the global power limited system produces a $\bar{P}/\hat{P}$ ratio of 0.9427, which is an improvement from the system with the local power limits which produced $\bar{P}/\hat{P} = 0.6070$. The instantaneous waveforms of these electrical powers when the power limit is $P_{MAX} = 0.25$ MW are shown in Fig. 8. Here the individual device power waveforms from both the local and global cases are shown along with the overall array power waveform showing the aggregation of all the three WECs connected onto the same DC bus. In the case of the local

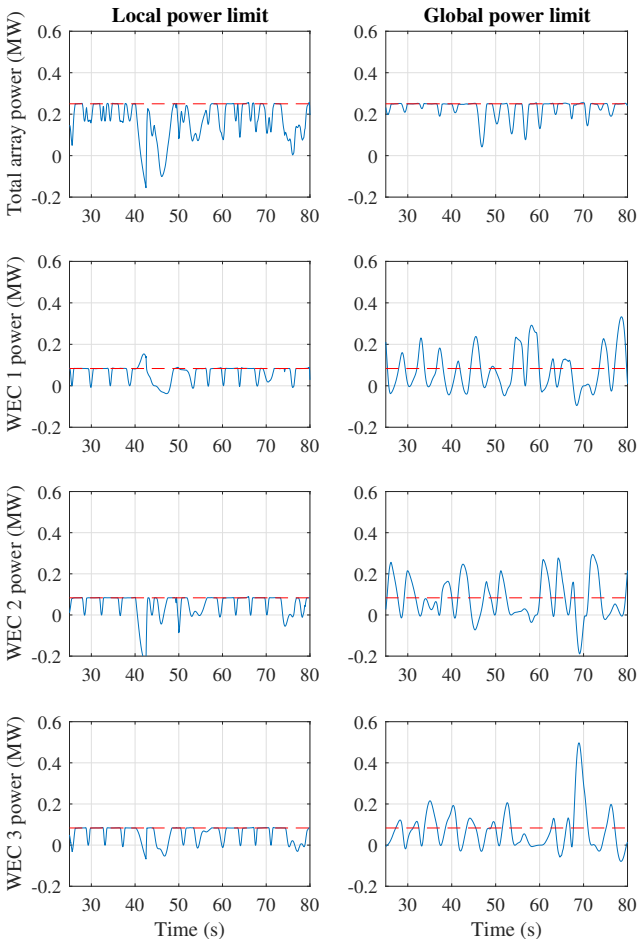

Fig. 8. Example waveforms of the system with the **Local power limit** and the **Global power limit** for a unidirectional irregular sea state modelled using a Bretschneider spectrum with $H_s = 3$ m and $T_s = 9.6$ s; for both modes the total aggregated power from the array and their corresponding instantaneous power waveform from each device are shown.

power limited system, it is clear that each WEC is constrained to operate underneath a certain power limit (0.0833 MW), hence leading to the overall power limit constraint of the array ($3 \times 0.0833 = 0.25$ MW). The global power limited system on the other hand operates in a different manner, where the aggressiveness of the local power from each device is permitted to be more oscillatory as long as the local linear constraints are upheld, hence explaining why the local power produced from each device breaches the local power limits but maintains the global power limit of the array. By choosing a moderate global power limit with the centralised NMPC, the average power may decrease, but this results in exceptional power quality that would significantly reduce the problems that would arise when exporting the power onto the grid.

Now, the sea state energy is increased to a higher level (using a Bretschneider excitation wave with $H_s = 5$ m and $T_s = 11$ s). The comparison between the globally and locally power limited system is shown in Fig. 9. As previously seen, the global power limited system produces higher average power $\bar{P}$ than the local power limited system for low values of the power limit P_{MAX}, as shown in Fig. 9(a). Examining

This article has been accepted for publication in a future issue of this journal, but has not been fully edited. Content may change prior to final publication. Citation information: DOI 10.1109/TSTE.2018.2812749, IEEE Transactions on Sustainable Energy

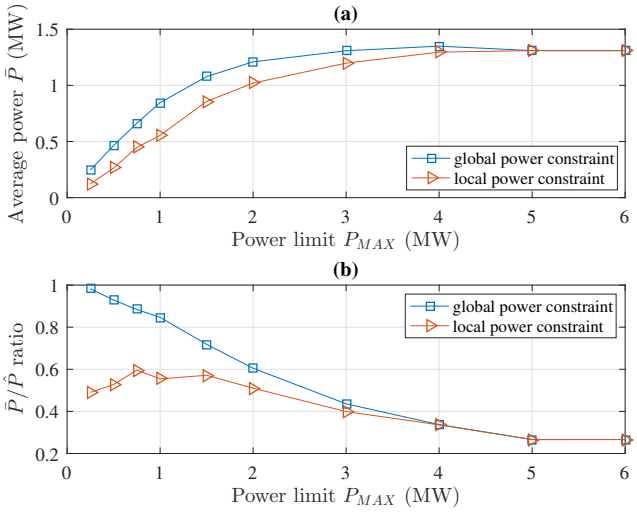

Fig. 9. The effect of either a global power constraint or a local power constraint on the power extracted from a three device array excited with a Bretschneider excitation wave with $H_s = 5$ m and $T_s = 11$ s (a) the average absorbed power $\bar{P}$ from the entire three WEC array, (b) the average to peak power ratio $\bar{P}/\hat{P}$ of the entire three WEC array

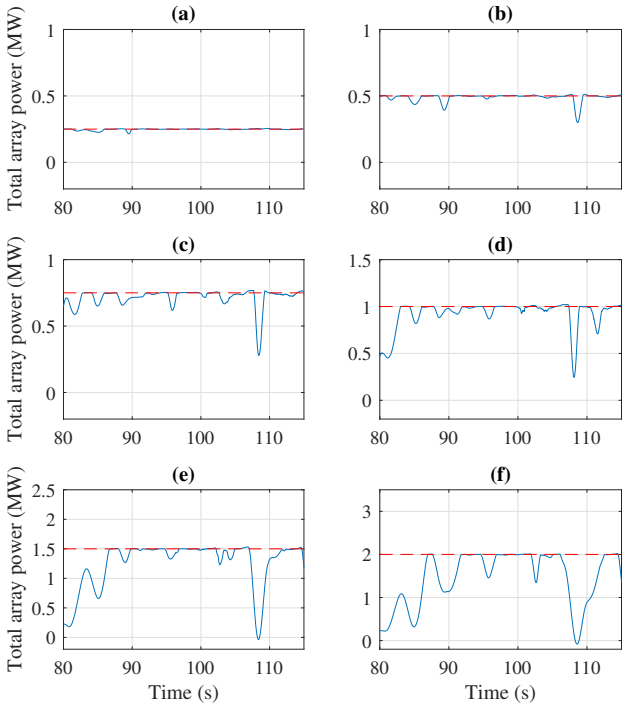

Fig. 10. Waveforms of the aggregated instantaneous power from the entire array using a Bretschneider excitation wave with $H_s = 5$ m and $T_s = 11$ s and the **Global power limit** of (a) 0.25 MW, (b) 0.5 MW, (c) 0.75 MW, (d) 1 MW, (e) 1.5 MW, (f) 2 MW.

the average to peak power ratio $\bar{P}/\hat{P}$ in Fig. 9(b), the benefits of choosing a global power limit over a local power limit is evident; especially for the lower power limit P_{MAX} range where the ratio $\bar{P}/\hat{P}$ is significantly better for the global (array) power constraint. When $P_{MAX} = 2$ MW is chosen, the global power constrained WEC array produces average powers that are 92.4% efficient when compared to the average power absorbed from the array without a global power constraint, while reducing the grid side converter rating by 59.3%. Therefore, the power quality is improved, the average power is sufficient and the grid side converter cost is reduced. Examples of instantaneous powers produced from the global power limited system with different power limits P_{MAX} are shown in Fig. 10. It is clear that as the global power limit P_{MAX} decreases, the instantaneous power becomes more constant.

V. Conclusion

This work was based on the premise that there was a benefit to be obtained from the centralised optimal control of interacting WECs. First, it was shown that when linear mechanical constraints and viscous effects were included in the optimisation problem, the variability of the absorbed average power from monochromatic waves in response to changes in the penetration angle reduced. This demonstrates an improvement in the robustness of the performance to array layout when the WECs undergo more realistic wave conditions.

With the inclusion of the linear constraints and the viscous forces in the MPC optimisation, the difference between the performances of the decentralised and the centralised MPC reduced. By exciting the system with multiple sea states with a range of separation distances, a comparison of the average power values absorbed between the centralised and decentralised MPCs was then made. It was shown that in general, if the separation distance of the WEC devices was low and the sea state was un-energetic, that the difference between the global and local MPC performance was more significant. This is due to the larger interaction when the WECs are closer together and the inactivity of the linear mechanical constraints.

It could be said that for a multi-body WEC system where the WECs are fixed to each other, the need for a centralised NMPC would be necessary because of their low d/r ratio. However, it could also be said that for WEC arrays with large WECs, the d/r ratio would practically need to be over a certain threshold to allow for maintenance and to reduce the probability of device collision. Hence for large WECs in an array, there may be little benefit in implementing a centralised NPMC.

Besides power maximisation, it is desirable that the control system can improve the average to peak power ratio and hence improve the power quality, the regulation of the DC-link and importantly lead to a reduction in the rating of the grid side converter. With the incorporation of an upper power limit on the power extracted either from each device, or from the complete array, it was shown that the average to peak power ratio could be increased by lowering the power constraint. The main highlight of this power quality analysis was the considerable difference in performance at lower power constraint levels when the power constraint was applied for the whole array rather than at each individual device. This demonstrated a potential benefit of using a global MPC approach. It is important to note that tightening the global power constraints for an array allows the user to improve the quality of power exported to the grid, at the cost of curtailed power. A full analysis of the benefits of this technique for improved power quality for weak grid connections, which focuses on flicker and total harmonic distortion would be helpful.

REFERENCES

[1] B. G. Cahill and T. Lewis, "Wave energy resource characterisation of the Atlantic Marine Energy Test Site," *International Journal of Marine Energy*, vol. 1, no. Supplement C, pp. 3–15, 2013.

[2] F. d. O. Antonio, "Wave energy utilization: A review of the technologies," *Renewable and sustainable energy reviews*, vol. 14, no. 3, pp. 899–918, 2010.

[3] M. Folley, A. Babarit, B. Child, D. Forehand, L. O'Boyle, K. Silverthorne, J. Spinneken, V. Stratigaki, and P. Troch, "A review of numerical modelling of wave energy converter arrays," *Proceedings of the 31st International Conference on Offshore Mechanics & Arctic Engineering, Rio de Janeiro, Brazil*, pp. 10–15, 2012.

[4] K. Thorburn, H. Bernhoff, and M. Leijon, "Wave energy transmission system concepts for linear generator arrays," *Ocean Engineering*, vol. 31, no. 11, pp. 1339–1349, 2004.

[5] H. Polinder, M. E. C. Damen, and F. Gardner, "Linear PM Generator System for Wave Energy Conversion in the AWS," *IEEE Transactions on Energy Conversion*, vol. 19, no. 3, pp. 583–589, 2004.

[6] A. Blavette, D. L. O'Sullivan, T. W. Lewis, and M. G. Egan, "Dimensioning the equipment of a wave farm: Energy storage and cables," *IEEE Transactions on Industry Applications*, vol. 51, no. 3, pp. 2470–2478, 2015.

[7] I. López, J. Andreu, S. Ceballos, I. M. de Alegr\'\ia, and I. Kortabarria, "Review of wave energy technologies and the necessary power-equipment," *Renewable and Sustainable Energy Reviews*, vol. 27, pp. 413–434, 2013.

[8] F. Bizzozero, S. Bozzi, G. Gruosso, G. Passoni, and M. Giassi, "Spatial interactions among oscillating wave energy converters: Electricity production and power quality issues," *Industrial Electronics Society, IECON 2016-42nd Annual Conference of the IEEE*, pp. 4235–4240, 2016.

[9] M. Santos-Mugica, D. B. Haim, F. Salcedo, and J. L. Villate, "Grid Integration of Wave Energy Farms: Basque Country Study," *3rd International Conference on Ocean Energy (ICOE2010)*, pp. 1–7, 2010.

[10] M. Göteman, J. Engström, M. Eriksson, and J. Isberg, "Optimizing wave energy parks with over 1000 interacting point-absorbers using an approximate analytical method," *International Journal of Marine Energy*, vol. 10, pp. 113–126, 2015.

[11] A. Babarit, "On the park effect in arrays of oscillating wave energy converters," *Renewable Energy*, vol. 58, pp. 68–78, 2013.

[12] P. B. Garcia-Rosa, G. Bacelli, and J. V. Ringwood, "Control-informed optimal array layout for wave farms," *IEEE Transactions on Sustainable Energy*, vol. 6, no. 2, pp. 575–582, 2015.

[13] A. Babarit, G. Duclos, and A. H. Clément, "Comparison of latching control strategies for a heaving wave energy device in random sea," *Applied Ocean Research*, vol. 26, no. 5, pp. 227–238, 2004.

[14] A. Babarit, M. Guglielmi, and A. H. Clément, "Declutching control of a wave energy converter," *Ocean Engineering*, vol. 36, no. 12, pp. 1015–1024, 2009.

[15] R. Nie, J. Scruggs, A. Chertok, D. Clabby, M. Previsic, and A. Karthikeyan, "Optimal causal control of wave energy converters in stochastic waves–Accommodating nonlinear dynamic and loss models," *International Journal of Marine Energy*, vol. 15, pp. 41–55, 2016.

[16] K. Budal and J. Falnes, "Optimum operation of improved wave-power converter," *Marine Science Communications*, vol. 3, pp. 133–150, 1977.

[17] E. Abraham and E. C. Kerrigan, "Optimal active control and optimization of a wave energy converter," *IEEE Transactions on Sustainable Energy*, vol. 4, pp. 324–332, 2013.

[18] G. Li, G. Weiss, M. Mueller, S. Townley, and M. R. Belmont, "Wave energy converter control by wave prediction and dynamic programming," *Renewable Energy*, vol. 48, pp. 392–403, 2012.

[19] G. Bacelli and J. V. Ringwood, "Numerical optimal control of wave energy converters," *IEEE Transactions on Sustainable Energy*, vol. 6, no. 2, pp. 294–302, 2015.

[20] J. A. M. Cretel, A. W. Lewis, G. Lightbody, and G. P. Thomas, "An Application of Model Predictive Control to a Wave Energy Point Absorber," *Proceedings of the IFAC Conference on Control Applications in Marine Systems*, no. 1980, pp. 1–6, 2010.

[21] A. C. M. O'Sullivan and G. Lightbody, "Co-design of a wave energy converter using constrained predictive control," *Renewable Energy*, vol. 102, pp. 142–156, mar 2017.

[22] ——, "The Effect of Viscosity on the Maximisation of Electrical Power from a Wave Energy Converter under Predictive Control, Toulouse, France," *The 20th World Congress of the International Federation of Automatic Control*, pp. 14 698–14 704, 2017.

[23] N. Faedo, S. Olaya, and J. V. Ringwood, "Optimal control, MPC and MPC-like algorithms for wave energy systems: An overview," *IFAC Journal of Systems and Control*, vol. 1, pp. 37–56, 2017.

[24] G. Bacelli, R. Genest, and J. V. Ringwood, "Nonlinear control of flap-type wave energy converter with a non-ideal power take-off system," *Annual Reviews in Control*, vol. 40, pp. 116–126, 2015.

[25] D. Oetinger, M. E. Magaña, and O. Sawodny, "Decentralized model predictive control for wave energy converter arrays," *IEEE Transactions on Sustainable Energy*, vol. 5, no. 4, pp. 1099–1107, 2014.

[26] M. Folley and T. J. T. Whittaker, "The effect of sub-optimal control and the spectral wave climate on the performance of wave energy converter arrays," *Applied Ocean Research*, vol. 31, no. 4, pp. 260–266, 2009.

[27] G. Bacelli and J. Ringwood, "Constrained control of arrays of wave energy devices," *International Journal of Marine Energy*, vol. 3, pp. 53–69, 2013.

[28] D. Oetinger, M. E. Magaña, and O. Sawodny, "Centralised model predictive controller design for wave energy converter arrays," *IET Renewable Power Generation*, vol. 9, no. 2, pp. 142–153, 2014.

[29] P. Mc Namara, R. R. Negenborn, B. De Schutter, and G. Lightbody, "Optimal coordination of a multiple HVDC link system using centralized and distributed control," *IEEE Transactions on Control Systems Technology*, vol. 21, no. 2, pp. 302–314, 2013.

[30] M. Diehl, T. Keviczky, B. De Schutter, and M. Doan, Dang, "A Jacobi Decomposotion algorithm for distribuated convex optimisation in distribuated model predicitive control," *120h IFAC World Congress*, 2017.

[31] W. E. Cummins, "The Impulse Response Function and Ship Motions," *Schiffstechnik*, vol. 9, pp. 101–109, 1962.

[32] J. Falnes, *Ocean Waves and Oscillating Systems: Linear Interactions Including Wave-Energy Extraction*. Cambridge University Press, 2002.

[33] C.-H. Lee, *WAMIT Theory Manual*, 1995.

[34] S.-Y. Kung, K. S. Arun, and D. V. B. Rao, "State-space and singular-value decomposition-based approximation methods for the harmonic retrieval problem," *JOSA*, vol. 73, no. 12, pp. 1799–1811, 1983.

[35] J. R. Morison, J. W. Johnson, S. A. Schaaf, and Others, "The force exerted by surface waves on piles," *Journal of Petroleum Technology*, vol. 2, no. 05, pp. 149–154, 1950.

[36] M. A. Bhinder, A. Babarit, L. Gentaz, and P. Ferrant, "Assessment of Viscous Damping via 3D-CFD Modelling of a Floating Wave Energy Device," *In Proceedings of the 9th European Wave and Tidal Energy Conference (EWTEC)*, pp. 1–6, 2011.

[37] Matlab, *Version 7.10.0*. Natick, Massachusetts: The MathWorks Inc., 2010.

[38] G. Li and M. R. Belmont, "Model predictive control of sea wave energy converters Part I: A convex approach for the case of a single device," *Renewable Energy*, vol. 69, pp. 453–463, 2014.

[39] T. Hürlimann, "AMPL: A mathematical programming language," *OR Spektrum*, vol. 15, no. 1, pp. 43–56, 1993.

[40] A. C. M. O'Sullivan and G. Lightbody, "The Effect of Model Inaccuracy and Move-blocking on the Performance of a Wave-to-wire Wave Energy Converter, under Economic Predictive Control," *In Proceedings of the 12th European Wave and Tidal Energy Conference (EWTEC)*, pp. 1–10, 2017.

Adrian C.M. O'Sullivan (S'17) received the BE (Hons) degree and the Ph.D. degree with MaREI from University College Cork (UCC), Cork, Ireland, in 2013 and 2018, respectively, both in electrical and electronic engineering. His research is based on decentralised and centralised model predictive control techniques on wave energy conversion systems, where the co-design from wave to wire is incorporated into the primary objective of maximising electrical power absorption.

Gordon Lightbody received the M.Eng. degree (with distinction) and the Ph.D. degree from Queens University, Belfast, U.K., in 1989 and 1993, respectively, both in electrical and electronic engineering. He is currently a Senior Lecturer with University College Cork, Cork, Ireland. His current research interests include artificial intelligence techniques for intelligent control and signal-processing, focusing on biomedical and energy/power applications. Dr. Lightbody is currently an Associate Editor with the Elsevier journal Control Engineering Practice.